TRAVELTIME TOMOGRAPHY IN ANISOTROPIC MEDIA

Jessé Costa

ABSTRACT

A stable reconstruction of anisotropic models from crosswell transmitted traveltimes is formulated and validated on synthetic data sets. The model is monoclinic and the symmetry plane is coincident with the acquisition plane. No approximation is used for the slowness surfaces and the raytracing is consistent with the model. The problem is ill-conditioned in consequence of the data type, *P*- and/or *S*-wave traveltimes, and the limited angular coverage provided by crosswell acquisition geometry. To recover meaningful results, regularization constraints are imposed requiring minimum anisotropy and inhomogeneity. Additional regularization is achieved controlling the scale of inhomogeneities allowed by parameterizing the model using nodes instead of cells. Application to the McElroy data set produced a virtually isotropic model.

INTRODUCTION

The broad angular ray coverage provided by crosswell surveys makes these experiments more sensitive to the occurrence of anisotropy than surface seismic experiments. The determination of the effective anisotropy at the crosswell frequency band has two important applications. Velocity models more consistent with traveltimes can improve the quality and likelihood of acoustic images. Besides, since effective anisotropy reflect patterns of inhomogeneities at scales much smaller than the dominant acoustic energy wavelength (Schoenberg & Muir, 1989), it can be potentially correlated, through geologic and petrophysical information, to the permo-porosity properties.

We present a stable algorithm to the reconstruction of anisotropic velocity models from traveltimes of q*P*- and/or q*S*v- transmitted waves. Previous approaches to this problem assumed approximations to the slowness surfaces. Cerveny (1982) derived the Frechét derivatives for traveltime inversion around an isotropic background. Chapman & Pratt (1992) and Pratt et al. (1993) investigated the limits of reconstruction for weak anisotropic models. Michelena et al. (1995) used the double-elliptical approximation (Dellinger et al., 1993) for transversally anisotropic models to justify the inversion of elliptical models in 1.5-D and posterior estimation of TI parameters. Costa et al. (1993) considered the inversion of 1-D transversally isotropic models and obtained an anelliptical model for the Devine data set.

We discuss the traveltime inversion for monoclinic models. The tomographic problem is formulated for arbitrary anisotropic slowness models and solved through linear iterations. The problem is then specialized to monoclinic models with a symmetry plane coincident with the acquisition plane. The limits of resolution of q*P*- and q*S*v-wave data are investigated and the subsets of parameters resolved by each data set are derived. The limited aperture of the crosswell experiment and the available data types, q*P*-and/or q*S*-waves, determine the nonuniqueness of the solutions, therefore defining an ill-posed problem (Menke, 1984). To obtain stable solutions, hopefully with geological meaning, the

solutions are constrained through three regularizing functionals (Menke, 1984). The first, functionl minimizes anisotropy in the solution. The other two, requiring solutions with minimum vertical and horizontal gradients, enforces homogeneity. The weight of the constraints on the solution decreases during the iterations following the continuation method proposed by Bube & Langan (1994). Additional regularization is obtained controlling the scale of heterogeneities by parameterizing the model using nodes (Harris, 1993). This algorithm is validated on synthetic data sets. The joint inversion of McElroy *P*- and *S*-wave transmitted traveltimes produced a virtually isotropic model.

THEORY

Model Parameterization

The traveltime of acoustic waves through an anisotropic elastic medium, under the framework of ray theory, is completely determined by the slowness surfaces at each point in the medium (Arnold, 1989). Besides the slowness surfaces obtained for anisotropic elastic medium from wave equation through plane wave (Musgrave, 1970) or asymptotic expansions (Cerveny, 1972), several approximations have been used in geophysics. The weak anisotropy approximation (Thomsen, 1986) was used by Stewart (1988). Chapman & Pratt (1992) also assume weak anisotropy. Michelena (1995) recovered transversally isotropic elastic parameters through traveltime inversion for elliptical models based on the double-elliptical approximation (Dellinger et al., 1993). We assume that the slowness surfaces in every point in the medium are defined by a dispersion relation in the form,

$$\mathrm{F}(\mathbf{s},\mathbf{x}) = \mathrm{F}(\mathbf{s},\eta(\mathbf{x})) = 0 \quad , \tag{1}$$

where, $\mathbf{x}$ is the position, $\mathbf{s}$ is slowness and η is the tensor of parameters defining the slowness surface. In order to trace rays through a model and set up the inversion problem we need a finite parameterization to $\eta(\mathbf{x})$. We use tensor products (DeBoor, 1978),

$$\eta(\mathbf{x}) = \sum_{i=1}^{nx}\sum_{j=1}^{nz}\eta_{ij}B_i(x-x_i)B_j(z-z_j) \quad , \tag{2}$$

where, η_{ij} is the tensor of parameters at $\mathbf{x}_{ij} \equiv (x_i, z_j)$, over a rectangular grid $n_x \times n_z$, B_i are the interpolation basis functions and $\mathbf{x} \equiv (x,z)$ is the position. Right now we are utilizing bilinear interpolation, but B-splines are being implemented.

Forward Modeling

The raypath connecting two points through a heterogeneous anisotropic medium is defined by the Fermat's Principle, which states that the traveltime is stationary along the ray trajectory in phase space, in this case, the extended space of position and slowness $(\mathbf{x},\mathbf{s})$. In mathematical language, the variation of the traveltime functional,

$$\tau = \int_{\mathbf{x}_0}^{\mathbf{x}_1} \mathbf{s}\cdot d\mathbf{x} \quad ,$$

subject to, (3)

$$\mathrm{F}(\mathbf{x},\mathbf{s}) = 0 \quad ,$$

should vanish along the ray. The solution of this variational problem results in the system of ordinary differential equations that governs the raypath and the slowness along the ray (Arnold, 1989),

$$\begin{aligned} \frac{d\mathbf{x}}{d\gamma} &= \lambda \nabla_s F \quad , \\ \frac{d\mathbf{s}}{d\gamma} &= -\lambda \nabla_x F \quad , \end{aligned} \tag{4}$$

where γ and λ depend on the specific parameterization for the raypath, for example, traveltime or path length. Two other equations are added to (4), one to integrate traveltime and another to integrate the dispersion relation (1) along the ray. This last equation is used to monitor the accuracy of the raytracing system. The resulting system of differential equations, using path length, l, as parameterization, is

$$\begin{aligned} \frac{d\mathbf{x}}{dl} &= \frac{\text{sign}(\mathbf{s}\cdot\nabla_s F)}{||\nabla_s F||}\nabla_s F \quad , \\ \frac{d\mathbf{s}}{dl} &= -\frac{\text{sign}(\mathbf{s}\cdot\nabla_s F)}{||\nabla_s F||}\nabla_x F \, , \\ \frac{d\tau}{dl} &= \frac{\text{sign}(\mathbf{s}\cdot\nabla_s F)}{||\nabla_s F||}\mathbf{s}\cdot\nabla_s F \, , \\ \frac{dS}{dl} &= F \, , \end{aligned} \tag{5}$$

with initial conditions,

$$\begin{aligned} &\mathbf{x}(l=0) = \mathbf{x}_0 \quad , \\ &F(\mathbf{x}_0, \mathbf{s}(l=0)) = 0 \, , \\ &\tau(l=0) = 0 \quad , \\ &S(l=0) = 1 \quad . \end{aligned} \tag{6}$$

This system is integrated using fourth order Runge-Kutta with controlled step size (Press et al., 1990). This integration scheme is accurate although more computationally expensive than fixed step size integration.

The two point raytracing is solved using the shooting method. We use an implementation developed by Robert Langan (personal comm.). An initial fan of rays with broad aperture is shot. If the desired end point is bracket by the fan, the algorithm performs a secant method search to find the required raypath. Otherwise, the fan is refined until it either brackets the end point or until it exceeds the maximum number of iterations allowed. This procedure is very robust and can capture multiple raypaths, in this case the raypath with minimum traveltime is used in the inversion.

Inverse Problem - Linearization

The reconstruction of $\eta(\mathbf{x})$ from crosswell traveltimes measurements is a nonlinear problem. The raypath depends on $\eta(\mathbf{x})$. One approach is to linearize the problem, computing the Fréchet derivative of the functional (3), and to proceed iteratively. Because traveltime along the ray is stationary, the time error resulting from the integration along a nearby, but erroneous raypath, distant from the actual ray by a small parameter of order ε, is of order ε^2. Thus when computing first order traveltime perturbations relative to changes in the parameters, $\delta\eta^p$, to first order in ε, from (3), traveltime does not vary with perturbation of the raypath, but only due to the perturbations in slowness. Thus one can write,

$$\delta\tau = \int_{ray} \sum_{i=1}^{N} \delta\eta^p \mathbf{s}_{,\eta^p} . \mathbf{x}' d\gamma \tag{7}$$

where the comma indicates partial derivatives, $\mathbf{x}' \equiv d\mathbf{x}/d\gamma$, and η^p represent the N_p components of the parameters tensor that defines the slowness surfaces. The total derivative of the dispersion relation (1) with respect to any particular η^p at any point $\mathbf{x}$ along the ray must vanish, i.e.,

$$\frac{d\,\mathrm{F}}{d\eta^p} = \mathrm{F}_{,\eta^p} + \mathbf{s}_{,\eta^p} \cdot \nabla_{\mathbf{s}} \mathrm{F} = 0 \tag{8}$$

From (4), $\mathbf{x}' = \lambda \nabla_{\mathbf{s}} \mathrm{F}$, substituting into the above equation gives,

$$\mathbf{s}_{,\eta^p} \cdot \mathbf{x}' = -\lambda \mathrm{F}_{,\eta^p} \quad , \tag{9}$$

and further substitution in (7), yields the result,

$$\delta\tau = - \int_{ray} \lambda \sum_{i=1}^{N} \mathrm{F}_{,\eta^p} \delta\eta_i d\gamma \quad . \tag{10}$$

Therefore, the derivative of the traveltime relative to η_{ij}^r for a model parameterized in the form (2), using the length along the ray as the integration variable, is given by,

$$\tau_{,\eta_{ij}^p} = - \int_{ray} \frac{\mathrm{sign}(\mathbf{s}.\nabla_{\mathbf{s}} \mathrm{F})}{\| \nabla_{\mathbf{s}} \mathrm{F} \|} \mathrm{F}_{,\eta_{ij}^p} B_i(x - x_i) B_j(z - z_j) dl \quad . \tag{11}$$

The determination of η_{ij} from a set of N_d measured traveltimes, τ_k^o, is performed iteratively. Starting from an initial model, $\eta = \lfloor \eta_{ij} \rfloor$, the raypath and the corresponding traveltime is computed for each source-receiver pair. The computed traveltimes, τ_k^c, yield a set of residuals, $\delta\tau_k$, that are approximated to first order by perturbations in the model parameters, $\delta\eta_{ij}^r$ by,

$$\delta\tau_k = \tau_k^o - \tau_k^c(\eta_{ij}^p) \approx \sum_i \sum_j \sum_p \tau_{,\eta_{ij}^p} \delta\eta_{ij}^p \quad , \tag{12}$$

a set of N_d equations in $n_x \times n_z \times N_p$ unknowns, $\delta\eta_{ij}^r$. After solving (12), the model is updated and the iteration repeated until the residual norm reaches a required tolerance level. In crosswell applications the system (12) is usually highly overdetermined, with N_d much greater than the number of unknowns, and the solution is obtained by least squares (Menke, 1984). However, although overdetermined, the linear system (12) is in general ill-conditioned (Lawson & Hanson, 1974). For tomography using isotropic models, this is due to the limited ray coverage provided by crosswell acquisition geometry (Spakman & Nolet,1988). The reconstruction of anisotropic models is even more unstable as discussed below.

Inverse Problem -Reconstruction Limits for Monoclinic Media

The most complex anisotropic model we consider is monoclinic with a vertical plane of mirror symmetry, plane X-Z, coincident with the acquisition plane. This model is the most general consistent with the 2-D nature of crosswell surveys. The tensor of density normalized elastic moduli for this model, in condensed notation (Musgrave, 1970), is

$$a_{IJ} = \begin{bmatrix} a_{11} & a_{12} & a_{13} & 0 & a_{15} & 0 \\ a_{12} & a_{22} & a_{23} & 0 & a_{25} & 0 \\ a_{13} & a_{23} & a_{33} & 0 & a_{35} & 0 \\ 0 & 0 & 0 & a_{44} & 0 & a_{46} \\ a_{15} & a_{25} & a_{35} & 0 & a_{55} & 0 \\ 0 & 0 & 0 & a_{46} & 0 & a_{66} \end{bmatrix} . \qquad (13)$$

For a medium whose elastic properties vary slowly with respect to the wavelength, the general dispersion relation which the slowness must satisfy at any point **x** (Musgrave, 1970) is

$$\mathrm{F}(\mathbf{x},\mathbf{s}) = \left| a_{ijkl}(\mathbf{x}) s_j s_l - \delta_{ik} \right| = 0 \quad , \qquad (14)$$

where, $a_{ijkl} \equiv c_{ijkl} / \rho$, is the density normalized elastic stiffness moduli, in indicial notation. At the symmetry plane of a monoclinic medium, represented by (13), the expression (14) can be factored in the form,

$$\mathrm{F}(\mathbf{s}) \equiv \mathrm{F}(s_1, s_3) = \mathrm{F}_{\mathrm{qP-qSv}}(\mathbf{s}) \times \mathrm{F}_{\mathrm{SH}}(\mathbf{s}) = 0 \quad , \qquad (15)$$

where,

$$\mathrm{F}_{\mathrm{SH}}(\mathbf{s}) = a_{66} s_1^2 + 2a_{46} s_1 s_3 + a_{44} s_3^2 - 1 = 0 \quad , \qquad (16)$$

and

$$\mathrm{F}_{\mathrm{qP-qSv}}(\mathbf{s}) = (a_{11} s_1^2 + a_{55} s_3^2 + 2a_{15} s_1 s_3 - 1)(a_{55} s_1^2 + a_{33} s_3^2 + 2a_{35} s_1 s_3 - 1) - \left[(a_{15} s_1^2 + a_{35} s_3^2 + 2(a_{13} + a_{55}) s_1 s_3\right]^2 = 0 \quad . \qquad (17)$$

The relation F_{SH} controls the slowness of *S*h-waves, i.e., waves with polarization perpendicular to the plane of propagation. The slowness of waves polarized along the symmetry plane, q*P*- and q*S*v-waves, are governed by (17). Since we are interested in q*P*- and q*S*v-waves inthe crosswellexperiment the slownesses considered from now on satisfy the dispersion relation (17). Consequently, the traveltimes of the q*P*- and q*S*v-waves that propagate along the symmetry plane of a monoclinic medium depend only on a_{11}, a_{13}, a_{15} , a_{33} , a_{35} , a_{55}. Our goal is therefore the reconstruction of these parameters in the region between the wells.

Equation (10) shows that the Fréchet derivatives of traveltime with respect to the dispersion relation parameters differ only by the derivatives of the dispersion relation itself with respect to η^{ν}. Thus, these derivatives controls the resolution of each parameter. First we investigate the limits of reconstruction of q*P*- and q*S*v-waves separately. To do this we introduce the following parameterization (Costa et al., 1993),

$$
\begin{aligned}
\eta_1 &\equiv C = \frac{a_{11}+a_{33}}{2} \ , \\
\eta_2 &\equiv c = a_{55} \ , \\
\eta_3 &\equiv D = \frac{a_{11}-a_{33}}{2} \ , \\
\eta_4 &\equiv \Delta = \frac{C-(a_{13}+2a_{55})}{2} \ , \\
\eta_5 &\equiv \psi = \frac{a_{15}+a_{35}}{2} \ , \\
\eta_6 &\equiv \varphi = \frac{a_{15}-a_{35}}{2} \ .
\end{aligned}
\tag{18}
$$

For an isotropic medium the only nonzero parameters are C and c, in this case, the square of *P*- and *S*-wave velocities respectively. The dispersion relation (17) takes the form,

$$
\begin{aligned}
\mathrm{F} = &\left[(C+D)s_1^2 + cs_3^2 + 2(\psi+\varphi)s_1s_3 - 1\right] \times \left[cs_1^2 + (C-D)s_3^2 + 2(\psi-\varphi)s_1s_3 - 1\right] - \\
&\left[(\psi+\varphi)s_1^2 + (\psi-\varphi)s_3^2 + (C-c-2\Delta)s_1s_3\right]^2 = 0
\end{aligned}
\tag{19}
$$

and the derivatives in (10) are,

$$
\begin{aligned}
\mathrm{F}_{,C} &= s^4\left[c + \Delta\sin^2 2\theta - \varphi\sin 4\theta - 1/s^2\right] \ , \\
\mathrm{F}_{,c} &= s^4\left[C + D\cos 2\theta - \Delta\sin^2 2\theta + 2\psi\sin 2\theta + \varphi\sin 4\theta - 1/s^2\right] \ , \\
\mathrm{F}_{,D} &= s^4\left[c\cos 2\theta - \frac{D}{2}\sin^2 2\theta + \frac{\psi}{2}\sin 4\theta - \varphi\sin 2\theta - 1/s^2\right] \ ,
\end{aligned}
\tag{20}
$$

$$F_{,\Delta} = s^4\left[2\psi\sin 2\theta + \varphi\sin 4\theta + (C - c - 2\Delta)\sin^2 2\theta\right] ,$$

$$F_{,\psi} = s^4\left[\frac{D}{2}\sin 4\theta - 2\psi\cos^2 2\theta - 2\varphi\cos 2\theta - 2(\Delta + c)\sin 2\theta - 2\sin 2\theta / s^2\right] ,$$

$$F_{,\varphi} = -s^4\left[D\sin 2\theta + (C - c - \Delta)\sin 4\theta + 2\psi\cos 2\theta + 2\varphi + 2\sin 2\theta / s^2\right] ,$$

where, $s = \sqrt{s_1^2 + s_3^2}$, and, $\theta = \mathrm{tg}^{-1}\left(\frac{s_3}{s_1}\right)$, is the slowness direction.

These partial derivatives can be interpreted using the weak anisotropy approximation discussed in Appendix A,

$$\begin{aligned} F_{qP_a}(\mathbf{s}) &\equiv \left[C + D\cos 2\theta - \Delta\sin^2 2\theta + 2\psi\sin 2\theta + \varphi\sin 4\theta - 1/s^2\right] = 0 , \\ F_{qSv_a}(\mathbf{s}) &\equiv \left[c + \Delta\sin^2 2\theta - \varphi\sin 4\theta - 1/s^2\right] = 0 . \end{aligned} \tag{21}$$

Comparing (21) and (20) we notice that,

$$F_{,C} = s^4 F_{qSv_a} \quad \text{and} \quad F_{,c} = s^4 F_{qP_a} \tag{22}$$

Thus,

- since, $F_{,c}$ is approximately zero for q*P*-waves, perturbations on this parameter cannot be recovered from q*P*-traveltimes irrespective of the angular ray coverage, at least in the f weak anisotropy limit.
- similarly, since $F_{,C}$ is almost zero q*S*v-waves so perturbations δC cannot be resolved from q*S*v-wave traveltimes.
- and, since the weak approximation for q*S*v-waves do not depend to first order on D and ψ, these parameter are poorly determined from q*S*v-wave traveltimes.

A related but somewhat weaker form of these results shows that only perturbations on a_{11}, a_{33} e $(a_{13} + 2a_{55})$ can be recovered from q*P*- traveltime data assuming weak anisotropy was described by Chapman & Pratt (1992).

Figure 1.a and 1.b are plots of the q*P*- and q*S*v-wave slowness curves and their corresponding weak anisotropy approximations for a medium with $D/C = 33\%$, $\Delta/C = 15\%$, $\psi = 0$ and $\varphi = 0$, i.e., a non-weak anisotropic medium. These plots indicate that, for values of anisotropy plausible for geologic materials, q*P*- traveltimes do not carry information on c and q*S*v-wave traveltimes do not depend on C, irrespective to the ray angular coverage through the medium. Another way of visualizing these results is by looking at the graphs of the dispersion relation (17) with respect to the parameters given by (18). These graphs are shown in Figures 2 and 3 for q*P*- and q*S*v-waves respectively.

These conclusions have implications as to the set up of the tomographic reconstruction for anisotropic models. One approach is to assume weak anisotropy and use the dispersion relations (21) for q*P*- and/or q*S*v-waves. As indicated by Figures 1.a and 1.b, these approximations are worse at the angular interval between 30° and 60°. In this work we do not use weak anisotropy and we assume that q*P*- and q*S*v-wave traveltimes are available.

Inverse Problem - Preconditioning

Another feature seen in Figures 2 and 3 is the strong angular dependence of the Fréchet derivatives. Thus, to obtain a stable reconstruction of anisotropic models a broad angular coverage is required throughout the medium. Unfortunately this coverage cannot be achieved in all regions of the model in crosswell surveys. The unavoidable limited aperture reduces the resolution and yields nonunique solution. This fact is translated numerically by the ill-conditioning of the tomographic system (12). To explicitly take into account the limited angular ray coverage and try to attenuate its dangerous effects the following parameterization is considered,

$$
\begin{aligned}
s_1^{-2} &\equiv s_{qP_a}^{-2}(0°) = C + D \ , \\
s_2^{-2} &\equiv s_{qP_a}^{-2}(30°) = C + \frac{D}{2} - \frac{3\Delta}{4} + \frac{\sqrt{3}}{2}(2\psi + \varphi) \ , \\
s_3^{-2} &\equiv s_{qP_a}^{-2}(-30°) = C + \frac{D}{2} - \frac{3\Delta}{4} - \frac{\sqrt{3}}{2}(2\psi + \varphi) \ , \\
s_4^{-2} &\equiv s_{qS_a}^{-2}(30°) = c + \frac{3\Delta}{4} - \frac{\sqrt{3}\varphi}{2} \ , \\
s_5^{-2} &\equiv s_{qS_a}^{-2}(-30°) = c + \frac{3\Delta}{4} + \frac{\sqrt{3}\varphi}{2}, \\
s_6^{-2} &\equiv s_{qS_a}^{-2}(0°) = c \ .
\end{aligned}
\tag{23}
$$

The motivation for the introduction of this parameterization is the preconditioning the tomographic system (12), since these parameters are associated with a limited angular sector of the slowness curves. To investigate the effect of this parameterization, the condition number (Lawson & Hanson, 1974) of the system (12) was computed for different values of angular ray coverage for two parameterizations defined by (18) and (23) respectively. The matrix of the tomographic system using *P*- and *S*v-wave traveltimes was computed for a homogeneous isotropic model with receivers placed in a circle around a source at 1° interval. The condition number for this matrix was computed using MATLAB. The results are shown in Table 1.

Angular Coverage	Parameters I	Parameters II
-90° - 90°	23.0072	13.7800
-60° - 60°	79.4686	16.2778
-30° - 30°	779.5074	129.3789

Table 1. Condition number of the tomographic system as a function of angular ray coverage. Parameters I are given by equations (18) and parameters II by equations (23).

This results show that parameterization II, equations (23), improves the condition number of the tomographic system. Although this result holds rigorously only for weak anisotropic models, since we linearized the problem around an isotropic model, we use this parameterization for the inversion qP- and qSv-wave traveltimes.

Inverse Problem - Regularization

The considerations above on the condition number of the tomographic system has a local character. The global resolution properties of the system (12) also depends strongly on the scale of heterogeneities allowed in the model. For isotropic models these aspects are discussed by Bube & Resnick (1984) and Spakman & Nolet (1988) who point out the low horizontal resolution of crosswell traveltime tomography. Michelena (1993), discussing the trade off of anisotropy and heterogeneity for elliptical models, shows that horizontal and high frequency variations in the vertical component of the slowness are poorly determined. These results indicate the importance of adding prior information on the scale of heterogeneities allowed in the model for regularizing inversion. Parameterizing the model in the form (2) improves the flexibility for controlling the scale of heterogeneities allowed. Since the tomographic problem is ill-posed, for all the reasons discussed above, we need to introduce regularization constraints (Menke, 1984). We use three regularizing functionals. The first requires that deviations from isotropy to be minimized. The other two penalize horizontal and vertical variations and therefore constrain against heterogeneity. The regularized problem takes the form,

$$\text{Minimize } \| \tau_{obs} - \tau_{calc}(\eta) \|_2^2 + \lambda_1^2 \| \mathbf{D}_{iso}\eta \|_2^2 + \lambda_2^2 \| \mathbf{D}_x\eta \| + \lambda_3^2 \| \mathbf{D}_z\eta \| , \quad (24)$$

where, τ_{obs}, is the measured traveltimes, τ_{calc} are the traveltimes through the model η and $\mathbf{D}_{iso}$, $\mathbf{D}_x$, $\mathbf{D}_z$ are first order finite difference operators that measure the variations in the model with respect to isotropy, horizontal, and vertical variations of the parameters respectively. The penalty parameters λ_1, λ_2 and λ_3 control the weight of each functional on the solutions with respect to fitting the data. The linearization of (24) yields the regularized tomographic system,

$$\begin{aligned} \mathbf{A}\delta\eta &= \delta\tau , \\ \lambda_1\mathbf{D}_{iso}\delta\eta &= -\lambda_1\mathbf{D}_{iso}\eta , \\ \lambda_2\mathbf{D}_x\delta\eta &= -\lambda_2\mathbf{D}_x\eta , \\ \lambda_3\mathbf{D}_z\delta\eta &= -\lambda_3\mathbf{D}_z\eta . \end{aligned} \quad (25)$$

The first set of equations corresponds to the system (12). At each iteration this linear system is solved using the conjugate gradient method for least squares (Spakman & Nolet, 1988).

Inverse Problem -Continuation Method

Equations (24) and (25) show that the parameters λ_1, λ_2 and λ_3 control the effectiveness of the regularization on the solution. The values of these parameters relative to the norm of the $\mathbf{A}$ matrix control the trade off between fitting the data and obeying the regularization constraints. In the continuation method (Bube & Langan, 1994), starting

from high values relative to the Frobenius norm of **A** matrix, the penalty terms are slowly relaxed over the iterations producing a family of solutions associated with the corresponding values of λ_1, λ_2 and λ_3. For each particular values of the penalty terms the linear iterations are performed until the norm of residuals in (25) does not decrease by a significant amount, this constitutes one step in the continuation method. Afterwards λ_1, λ_2 and λ_3 are decreased and the continuation step repeated. These continuation iterations proceed until the instabilities in (25) produce models so rough that the two point raytracing breaks down. A particular solution can then be singled out observing the trade off between fitting the data and obeying the regularization constraints.

APPLICATION TO SYNTHETIC DATA SETS

The algorithm was validated on two synthetic data sets. The synthetic models are based on the McElroy sonic log. One is isotropic and the other has anisotropy in one layer. The traveltimes for *P*- and *S*-waves were obtained using an eikonal finite difference approach for the isotropic model and the raytracing described in this paper for the anisotropic model. To try to mimic actual conditions data with a vertical offset less than 30 ft were masked. This is because the peizoelectric source radiation pattern do not generate *S*-waves in this direction. This also helps to minimize artifacts due to head waves that can occur in real data. The acquisition geometry is the same, the well distance is 200 ft and sources and receivers are spaced every 5 ft. These two data sets were inverted for a monoclinic model with 2x91 nodes distributed regularly every 5 ft in each well. The initial model is isotropic and homogeneous with Vp = 18.2 kft/s and Vs = 10.4 kft/s. The initial values of the penalty parameters λ_1, λ_2 and λ_3 relative to the Frobenius norm of the tomographic system (12) were 3, 3 and 0.75 respectively, therefore isotropic layered solutions are heavily weighted at the beginning of iterations. After each continuation step the penalty terms are divided by $\sqrt{10}$. The inversion results for the isotropic model data set, after 9 continuation steps, are shown in Figures 4 and 5. These plots show the velocities corresponding to the slowness parameters s_1, s_2, s_3, s_4, s_5 and s_6. The inverted model fits the data with an rms error of 16 microseconds. Figures 6 and 7 show the results after 10 continuation steps. The inversion results for the anisotropic model data set are shown in Figures 6 and 7, after 10 continuation steps. The inverted model fits the data with rms error of 20 microseconds. The artifacts near sharp boundaries are probably due to the use of bilinear interpolation which produces discontinuities in the gradient thus violating the assumptions of our raytracing. The inversion results for these synthetic data sets indicate that the algorithm proposed is stable, at least for the scale of heterogeneities allowed in these models.

APPLICATION TO MCELROY DATA SET

The next step was to apply the algorithm to the McElroy data set. The details of the acquisition can be found in Harris et al. (1995). The well head distance is 184 ft. Source and receiver positions were corrected to account for well deviations following Harris (1993). Due to memory limitation only a subset of 83 sources and 80 receivers were used. Data with vertical offset less than 30 ft were masked since the source radiation pattern does generate strong *S*v-waves (Van Schaack et al., 1995) at this interval and to avoid possible artifacts due to *P*-wave headwaves.

The data were inverted for a monoclinic model with 2x91 nodes discretized on a rectangular grid with 200 ft horizontal spacing and 5 ft vertical. The initial model was the same one used for the synthetic data sets with Vp = 18.2 kft/s and Vs = 10.4 kft/s. The penalty terms λ_1, λ_2 and λ_3 start with values 3, 3 and 0.75 respectively, relative to the Frobenius norm of the tomographic matrix in (12). After each continuation step these parameter are divided by $\sqrt{10}$. The profiles of the velocities corresponding to the

parameters in (23), after 8 continuation steps, are shown in Figures 8 and 9. The depths have been changed for presentation purposes. This model fits the data with an rms error of less than 150 microseconds for *P*-wave traveltimes and 300 microseconds for *S*-wave traveltimes, which is approximately equal to the picking error.

Figures 8 and 9 show that the inverted model does not present significant anisotropy. The differences between the profiles near sharp boundaries are probably due to the use of bilinear interpolation as pointed out earlier. Therefore, these results indicate that an isotropic medium is consistent with the McElroy data set. This result differs from Michelena et al. (1995) who obtained an anisotropic model for McElroy. About this we can only point out some differences favoring our approach. We think that the joint inversion of q*P*- and q*S*-wave traveltimes is a better constrained problem when inverting for anisotropic models. We also used a larger aperture since we were not constrained by the elliptical approximation. Finally, smooth models are more robust for traveltime tomography.

CONCLUSIONS

The reconstruction of anisotropic models from q*P*- and/or q*S*v-wave traveltimes was discussed. The resolution limits for the reconstruction of monoclinic media were derived and the effects of limited angular ray coverage were taken explicitly into account. The model was parameterized using nodes which permitted a flexible way to handle the trade off between anisotropy and heterogeneities. An accurate forward modeling raytracing code, consistent with the node parameterization, was developed which allows us to approach the nonlinear problem of tomographic reconstructions through linear iterations. The regularization of the tomographic system, through the minimization of anisotropy and heterogeneity on the solution, yields a stable algorithm, which was validated on synthetic data sets. The joint inversion of McElroy *P*- and *S*-wave traveltimes resulted in a virtually isotropic model.

The formulation presented is general and thereby any approximation for the slowness curves can be easily be included. The next steps in this project includes the extension of this approach to reflection traveltime tomography together with Mark Van Schaack. The reflection trajectories increase the ray angular coverage therefore reducing the null space of the tomographic system. The investigation of better ways to take advantage of the node parameterization as *a priori information* constraints is also a topic for future investigation.

ACKNOWLEDGMENTS

The field data were picked and edited by Mark Van Schaack. The first author strongly acknowledges Mark for his friendship and the great synergetic interaction in the work during this year. We also acknowledge Bob Langan and Ken Bube for sharing with us their continuation method code. Thanks to the Brazilian CNPq and all the sponsors of the Stanford Tomography Project that supported the first author this year in Stanford.

REFERENCES

Arnold, V. A., 1989, **Mathematical Methods of Classical Mechanics**. New York, Springer-Verlag. 508p. (Graduate Texts in Mathematics, 60).

Bube, K. P. & Langan, R. T., 1994, A continuation approach to regularization for traveltime tomography: Expanded Abstracts, SEG, **64**, 980-983.

Bube, K. P. & Resnick, J. R., 1984, Well-determined and poorly-determined features in seismic tomography: Expanded Abstracts, SEG, **54**, 717-719.

Cerveny, V., 1972, Seismic rays and ray intensities in inhomogeneous anisotropic media: Geophys. J. Roy. Astr. Soc., **29**, 1-13.

Cerveny, V., 1982, Direct and inverse kinematic problem for inhomogeneous anisotropic media-linearization approach: Contr. Geophys. Inst. Slov. Acad. Sci., **13**, 127-133.

Chapman, C. H. & Pratt, R.G., 1992, Traveltime tomography in anisotropic media. I-theory: Geophys. J. Int., **109**, 1-19.

Costa, J. C., Miller, D. Schoenberg, M., 1993, Ray tracing and tomography in anisotropic layered media-theory and practice, with application to Devine data set: Scientific Report Schlumberger Cambridge Research.

Costa, J. C., 1993, Modelagem sísmica e inversão na presença de anisotropia: Tese de Doutoramento. Depto. de Geofísica, UFPa.

Dellinger, J., Muir, F. & Karrenbach, M., 1993, Anelliptic approximations for TI media: J. Seismic Expl., **2**, 23-40.

Harris, J. M., 1993, Lattice parameterization for tomography: STP Annual Report, 4(1). Paper E.

Harris, J. M., Nolen-Hoeksema, R. C., Langan, R. T., Van Schaack, M., Lazaratos, S. K., & Rector III, J. W., High-resolution crosswell imaging of a west Texas carbonate reservoir: Part I - Project summary and interpretation: Geophysics, **60**, 667-681.

Helbig, K. & Schoenberg, M., 1987, Anomalous polarization of elastic waves in transversally isotropic media: J.Acoust. Soc. Am., **81**, 1235-1245

Menke, W., 1984, **Geophysical data analysis: discrete inverse theory**: New York, Academic Press. 206p.

Michelena, R. J.,1993, Anisotropic traveltime tomography: Ph.D thesis, Stanford University.

Michelena, R. J.,1995, Crosswell tomographic estimation of elastic constants in transversely isotropic media: Geophysics, **60**, 774-783.

Miller, D. & Chapman, C.H., 1991, Incontrovertible evidence of anisotropy in crosswell data: Expanded Abstracts, SEG, **61**, 825-828.

Musgrave, J. P., 1970, **Crystal acoustics**. Lodon, Holden-Day.288p.

Press, W.H, Flannery, B. P., Teukolsky, S. A. & Vetterling, W.T., 1990, **Numerical Recipes**. Cambridge. Cambridge University Press. 702p.

Van Schaack, M. A., Harris, J. M., Rector III, J. W. & Lazaratos, S. K., 1995, High-resolution crosswell imaging of a west Texas carbonate reservoir: Part 4-reflection imaging: Geophysics, **60**, 602-691.

Spakman, W. & Nolet, G., 1988, Imaging algorithms, accuracy and resolution in delay time tomography: In: **Mathematical Geophysics**. Editors: Vlaar, N.J. Nolet, G. Wortel, M.J.R. & Cloetingh, S.A.P.L. Dordretcht, D. Reidel Publishing Company. 407p.

Stewart, R. R., 1988, An algebraic reconstruction technique for weakly anisotropic velocity: Geophysics, **53**, 1613-1615.

Thomsen, L., 1986, Weak elastic anisotropy: Geophysics, **51**, 1954-1966.

APPENDIX A

APPROXIMATE SLOWNESS CURVES

Consider a arbitrary rotation in the plane X-Z, forming an angle α with respect to the X axis; the parameters (18) are transformed according to,

$$\begin{aligned} C' &= C - \Delta\sin^2 2\alpha + \varphi\sin 4\alpha \ , \\ D' &= D\cos 2\alpha + 2\psi \sin 2\alpha \ , \\ \Delta' &= \Delta\cos 4\alpha - \varphi\sin 4\alpha \ , \\ \psi' &= \psi\cos 2\alpha + \frac{D}{2}\sin 2\alpha \ , \\ \varphi' &= \varphi\cos 4\alpha - \frac{\Delta}{2}\sin 4\alpha \ , \\ c' &= c + \Delta\sin^2 2\alpha - \varphi\sin 4\alpha \ . \end{aligned} \tag{A-1}$$

For transversally isotropic media with symmetry axis in the plane or if the plane is coincident with the symmetry planes of an orthorhombic medium it is always possible to find a coordinate system such that ψ' and φ' vanish. In this system of principal axes the dispersion relation (19) takes the form

$$(s^{-2})^2 - (C + D\cos 2\theta + c)s^{-2} + c(C + D\cos 2\theta) + [(C - c)\Delta - \Delta^2 - \frac{D^2}{4}]\sin^2 2\theta = 0 \ , \tag{A-2}$$

a quadratic equation in s^{-2} (where s is the magnitude of the slowness vector) with coefficients that are functions of θ, the phase angle. The dispersion relation can be exactly factored (with an elliptical slowness curve for q*P*-waves and a circular q*S*v-wave slowness curve) if the quantity,

$$E^2 \equiv (a_{11} - a_{55})(a_{11} - a_{55}) - (a_{11} - a_{55})^2 = 4(C - c)\Delta - 4\Delta^2 - D^2 \ , \tag{A-3}$$

is equal to zero (Helbig & Schoenberg, 1987). Solving (A-2) gives q*P*- and q*S*v-waves,

$$s^{-2} = \frac{C + D\cos 2\theta + c}{2} \pm \sqrt{\left(\frac{C + D\cos 2\theta - c}{2}\right)^2 - \frac{E^2}{4}\sin^2 2\theta} \ . \tag{A-4}$$

Expanding these solutions in powers of the anisotropy parameters, D and Δ, and neglecting terms of order $O[D^2/(C-c)\ ,\ \Delta^2/(C-c)\ ,\ D\Delta/(C-c)]$, yield the simple expressions for phase slowness,

$$s^{-2}_{qP_a} \approx C + D\cos 2\theta - \Delta\sin^2 2\theta \ , \qquad s^{-2}_{qS_a} \approx c + \Delta\sin^2 2\theta \ . \tag{A-5}$$

which reconverted to a coordinate system noncoincident with the principal axes takes the form of (21).

The anellipticity parameter ε_A (Costa et al., 1993) (a nondimensional version of E^2, normalized so that $Max\ \varepsilon_A = 1$), becomes proportional to Δ in the weak approximation:

$$\varepsilon_A \equiv \frac{E^2}{(a_{11}-a_{55})(a_{33}-a_{55})} = \frac{4(C-c)\Delta - 4\Delta^2 - D^2}{(C-c)^2 - D^2} \approx \frac{4\Delta}{(C-c)} \quad . \qquad \text{(A-6)}$$

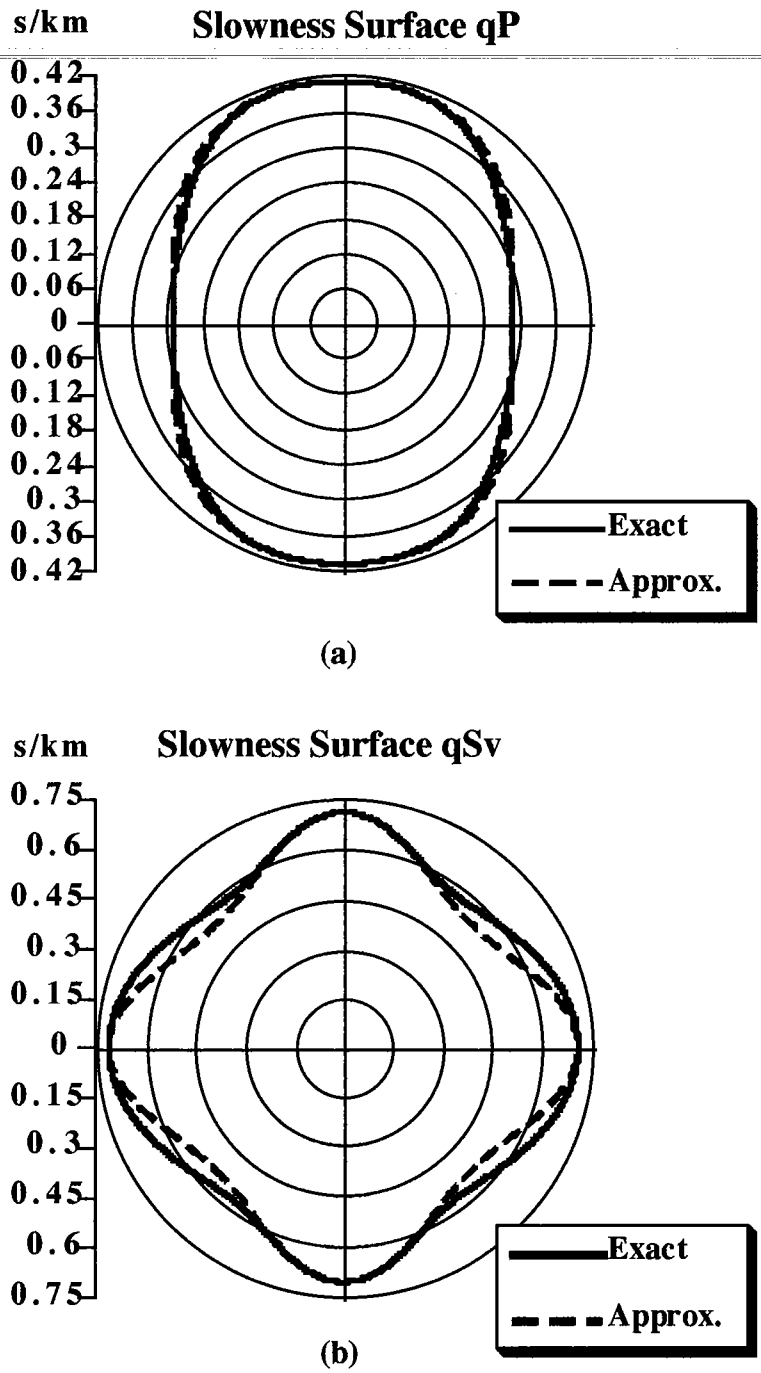

Figure 1: Slowness curves for q*P*- and q*S*v-waves and their corresponding weak anisotropy approximations calculated for a medium with parameters set as follows: $D/C = 33\%$, $\Delta/C = 15\%$ and $c/C = 2/9$. Even for this non-weak anisotropic medium the approximations are accurate, especially for the q*P*-wave slowness curve.

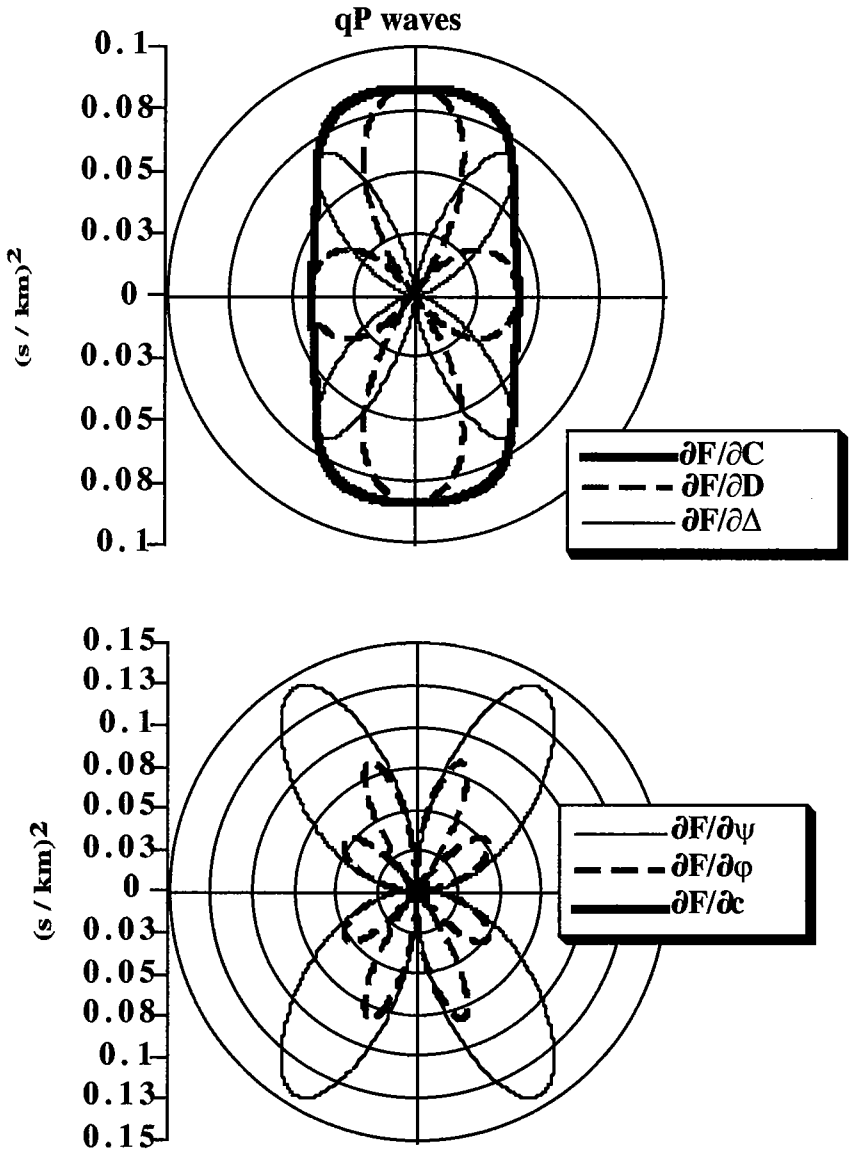

Figure 2: Derivatives of the dispersion relation with respect to the parameters (18) for q*P*-waves (equation 19) for the medium shown in Figure 1. The derivative $\partial F/\partial c$ can be neglected with respect to the others, even for this non weak anisotropic medium, indicating that this parameter cannot be recovered from q*P*-traveltimes.

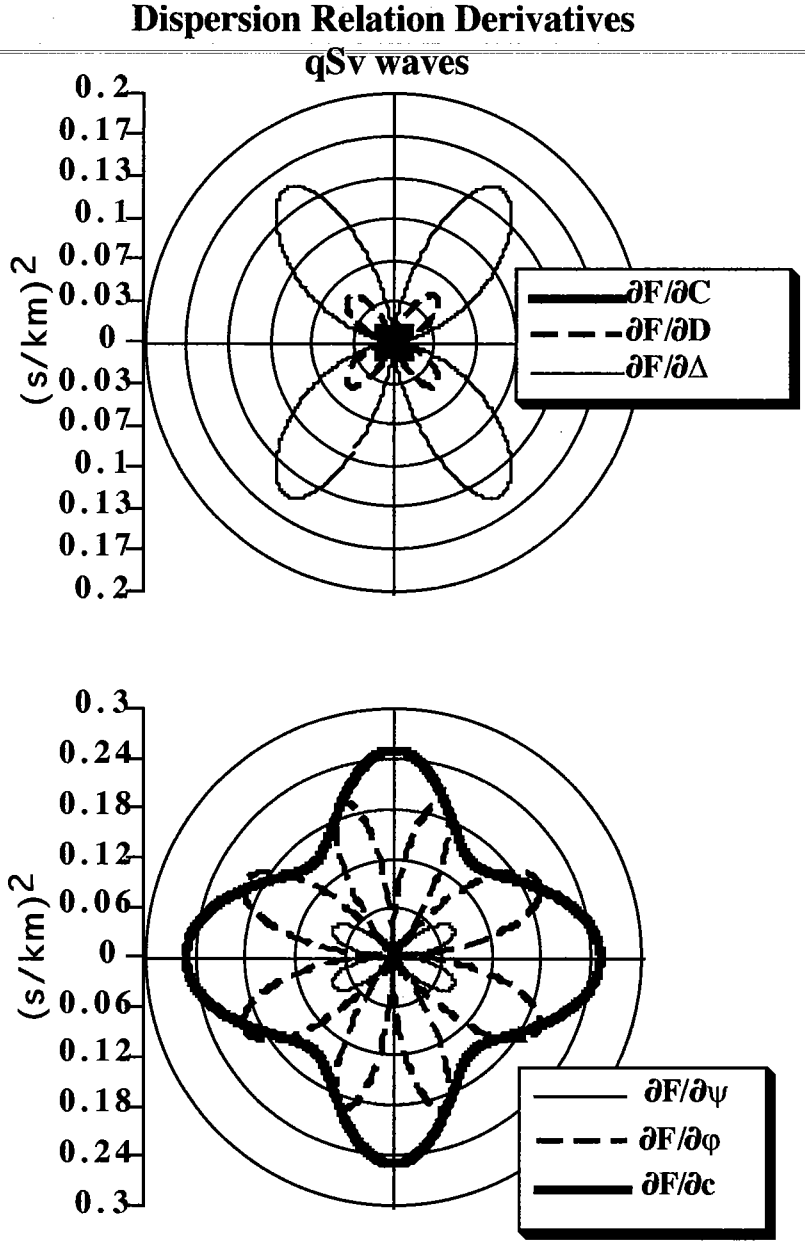

Figure 3: Derivatives of the dispersion relation for qSv-waves, equation (19), for the model shown in Figure 1. Notice that $\partial F/\partial C$ can be neglected with respect to the other derivatives indicating that this parameter cannot be recovered from qSv-wave traveltimes.

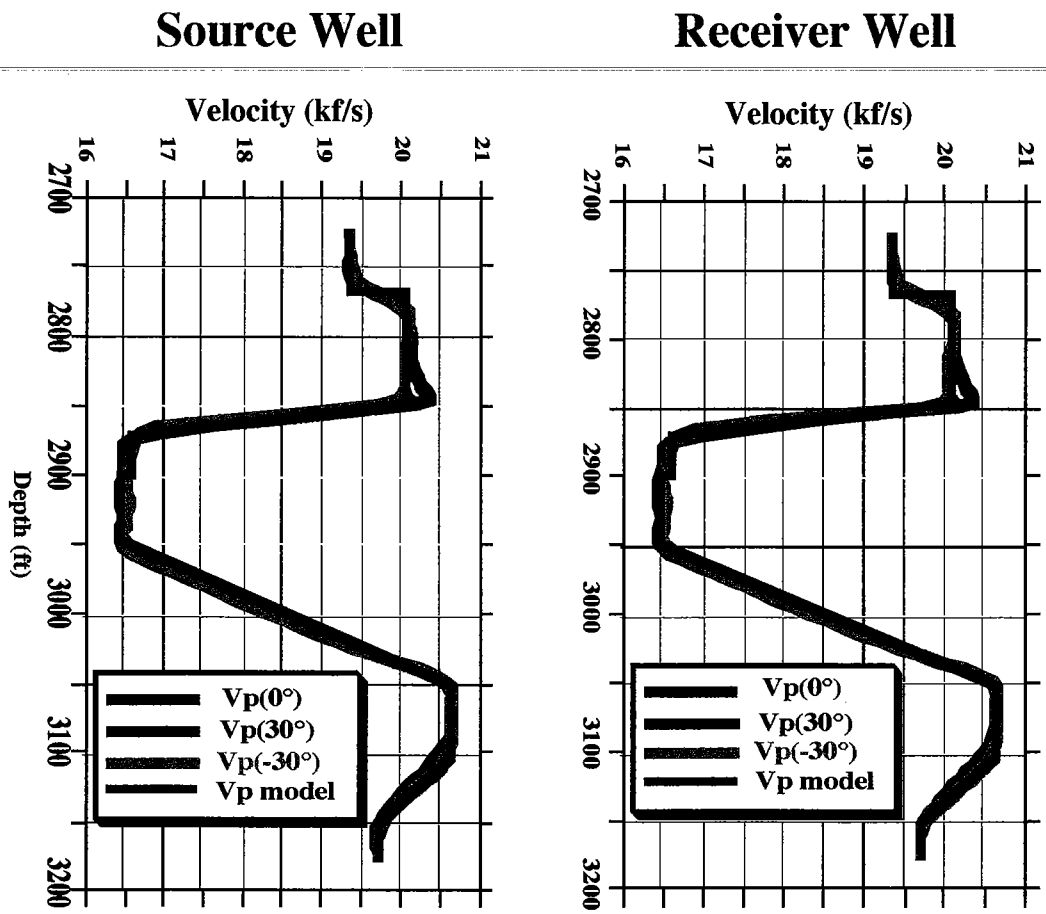

Figure 4: Profile of q*P*-velocity parameters, equation (23), after the inversion of the synthetic data set.

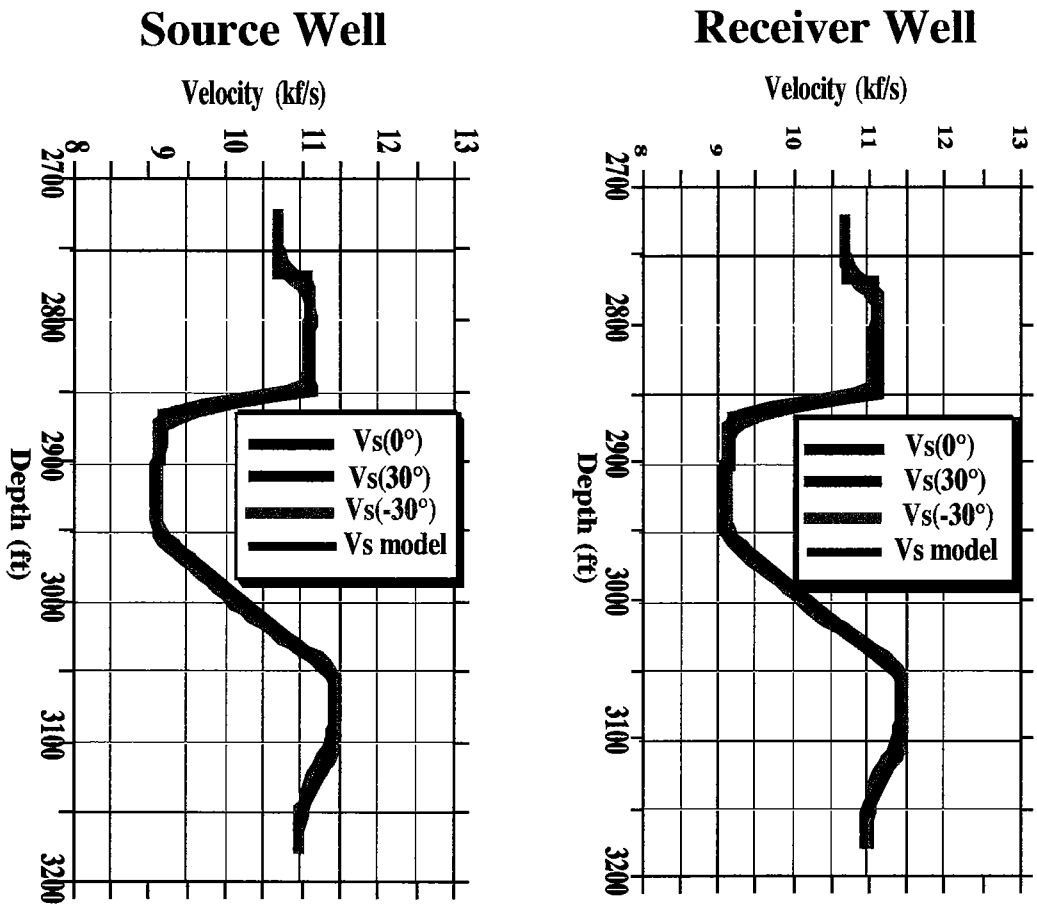

Figure 5: Profile of qSv-wave velocity parameters, equation (23), after the inversion of synthetic the data set.

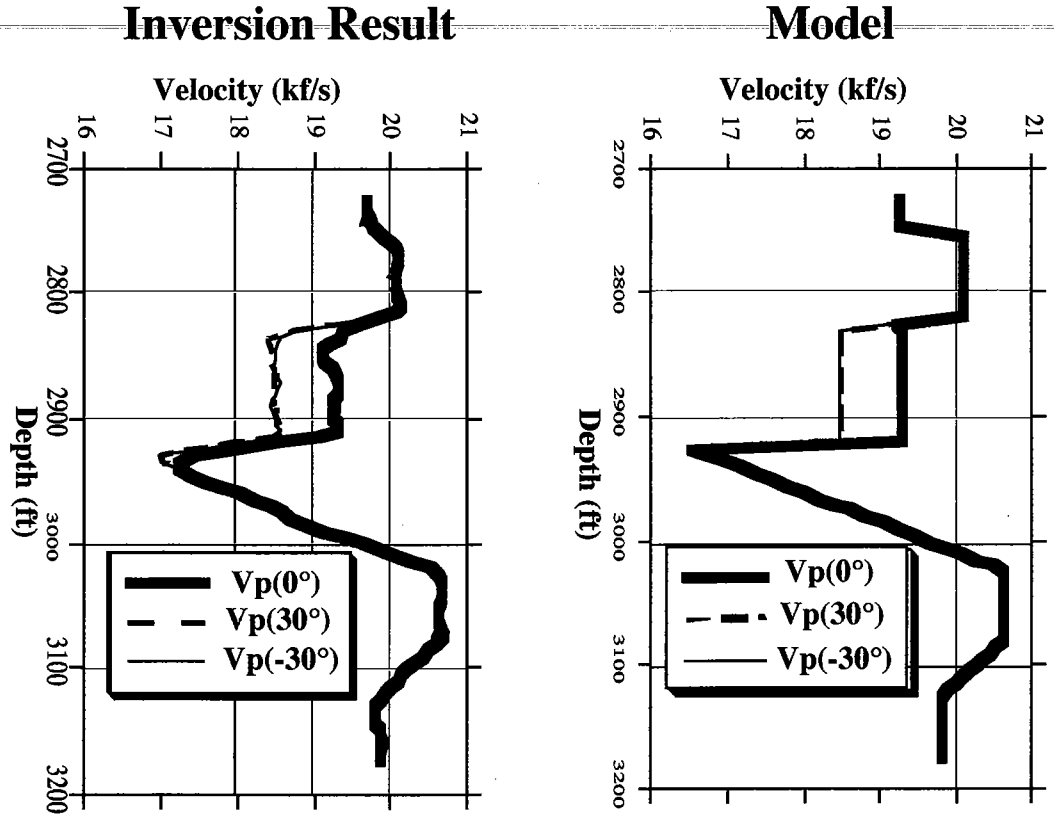

Figure 6: Profile of q*P*-velocity parameters, equation (23), after inversion of synthetic data set.

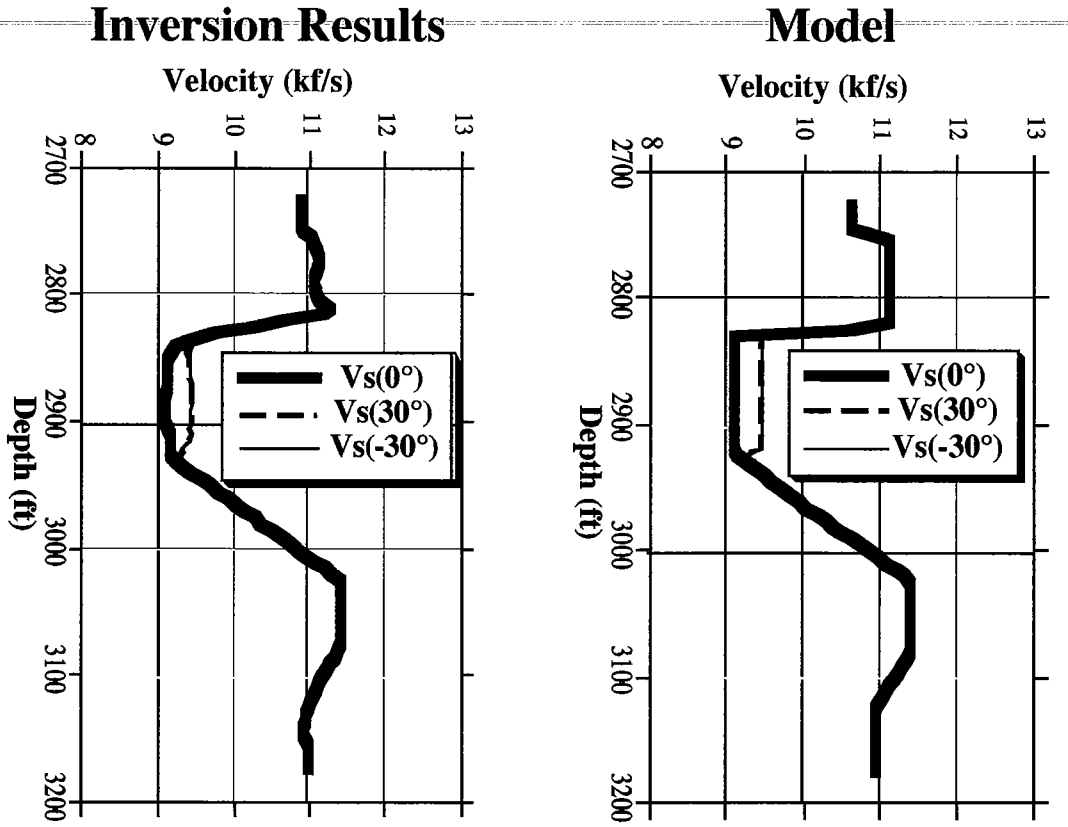

Figure 7: Profiles of the q*S*v-wave velocity parameters, equation (23), after the inversion of the synthetic data set.

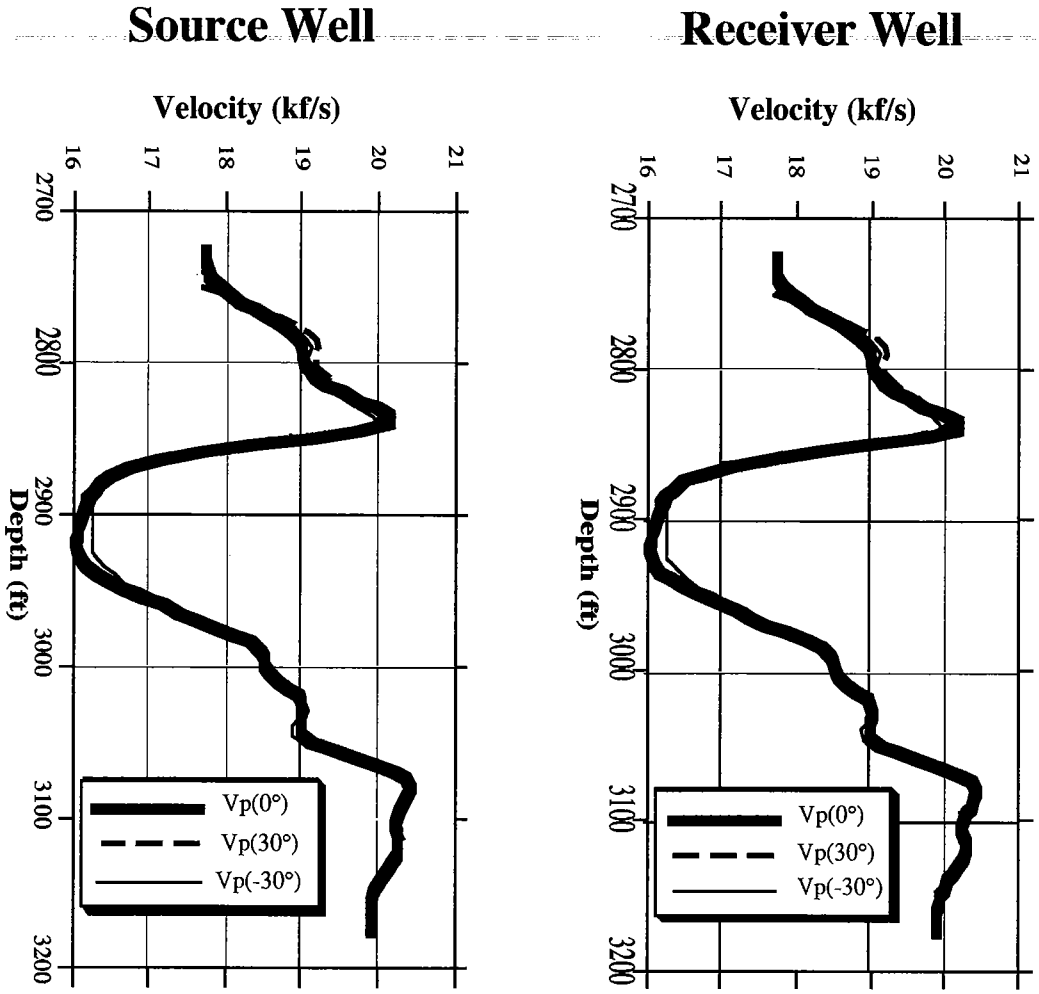

Figure 8: q*P*- velocity parameters, equation (23), after joint inversion of *P*- and *S*v-wave McElroy traveltimes.